Mathematical Biosciences 270 (2015) 106–114

Contents lists available at ScienceDirect

Mathematical Biosciences

journal homepage: www.elsevier.com/locate/mbs

Prediction of *in-vivo* iontophoretic drug release data from *in-vitro* experiments–insights from modeling

Laurent Simon [a,*], Juan Ospina [b], Kevin Ita [c]

[a] Otto H. York Department of Chemical, Biological and Pharmaceutical Engineering, New Jersey Institute of Technology, Newark NJ 0702, USA
[b] Logic and Computation Group, Physics Engineering Program, School of Sciences and Humanities, EAFIT University, Medellin, Colombia
[c] College of Pharmacy, Touro University Mare Island-Vallejo, California 94592, USA

ARTICLE INFO

Article history:
Received 18 April 2015
Revised 4 October 2015
Accepted 16 October 2015
Available online 2 November 2015

Keywords:
Iontophoresis
In-vivo in-vitro correlation
Laplace transform
Controlled release
Closed-form solution

ABSTRACT

A strategy was developed to predict *in-vivo* plasma drug levels from data collected during *in-vitro* transdermal iontophoretic delivery experiments. The method used the principle of mass conservation and the Nernst–Planck flux equation to describe molecular transport across the skin. Distribution and elimination of the drug in the body followed a one- or two-compartment open model. Analytical expressions for the relaxation constant and plasma drug concentration were developed using Laplace transforms. The steady-state dermal flux was appropriate for predicting drug absorption under *in-vivo* conditions only when the time constant in the skin was far greater than its value in the blood compartment. A simulation study was conducted to fully assess the performance of estimations based on the equilibrium flux approximation. The findings showed that the normalized integral of squared error decreased exponentially as the ratio of the two time constants (blood/skin) increased. In the case of a single compartment, the error was reduced from 0.15 to 0.016 when the ratio increased from 10 to 100. The methodology was tested using plasma concentrations of a growth-hormone releasing factor in guinea pigs and naloxone in rats.

1. Introduction

The transdermal route is used to introduce a number of medications into the body. However, serious challenges remain because of the low skin permeability caused by the stratum corneum, the outermost layer of the epidermis [1]. Several strategies are available for increasing transdermal drug delivery including sonophoresis, chemical penetration enhancers, microneedles and iontophoresis [2,3,4,5]. The latter technique represents a noninvasive method by which a mild electric current ($\leq$0.5 mA/cm^2) is used to increase percutaneous penetration of ionized drugs [5]. According to this method, the medication is applied to an electrode carrying a similar charge. The oppositely charged electrode is inserted in a different location of the body, inducing the current to flow. Advantages of iontophoresis include ease of application, minimal side effects and increased permeability, making it a common procedure employed for transdermal drug delivery [6]. Cations are placed in the anodal compartment and anions in the cathodal compartment. The repulsion of cations from the anode, or anions, from the cathode ensures that drug ions are delivered into and through the skin. There are other mechanisms involved in iontophoresis including electroosmosis and increased skin permeability [7]. Electroosmosis occurs due to the negative charge of the skin at physiological pH. This process increases percutaneous transport of neutral and positively- charged molecules in the anode-to-cathode direction [5].

Major efforts are underway to develop better *in-vivo in-vitro* correlations (IVIVCs). Nugroho et al. created compartmental models to describe *in-vitro* iontophoretic transport [8]. Their empirical approach was based on a mass-transfer interpretation of the process and included parameters, such as a kinetic lag time, steady-state flux and a first-order rate constant for iontophoresis. The derived equations were fitted to apomorphine and rotigotine iontophoretic delivery data. A similar compartmental framework was provided to explain *in-vivo* iontophoretic delivery of the growth hormone-releasing factor (GRF), R-apomorphine and alniditan [9]. A constant or time-varying input represented the transdermal flux. Elimination from the systemic circulation was described by one- or two-compartment pharmacokinetics.

Initial attempts to derive IVIVCs during iontophoresis [9] have notable merits. Compartment mass-transfer models allow, in some cases, accurate predictions of *in-vivo* performance based on data collected in *in-vitro* investigations. The compartmental approach developed in [9] reveals that the predictive capability of the *in-vivo* model increases when a transient transdermal flux is used. These findings mark a departure from earlier contributions which assumed that the drug input into the systemic circulation was held constant during

* Corresponding author. Tel.: +1 973 596 5263; fax: +1 973 596 8436.
E-mail address: laurent.simon@njit.edu (L. Simon).

http://dx.doi.org/10.1016/j.mbs.2015.10.011
0025-5564/

Nomenclature

A	surface area of the transdermal patch
C	concentration of drug in the skin
C_1	drug concentration in the central compartment of a two-compartment model
$\bar{C}_1$	Laplace transform of C_1
C_2	drug concentration in the peripheral compartment of a two-compartment model
$\bar{C}_2$	Laplace transform of C_2
C_p	plasma drug concentration
$\bar{C}_p$	Laplace transform of C_p
Cp_{stead}	predicted plasma drug concentration based on the steady-state flux (i.e., Eq. (34) or Eq. (49))
Cp_{trans}	predicted plasma drug concentration based the transient flux (i.e., Eq. (31) or Eq. (44))
C_s	surface concentration at the skin-vehicle interface
C_{ss}	steady-state plasma drug concentration
CL_t	the total body clearance
D	drug diffusivity in the skin
f	generic monotonic function
$\bar{F}$	Laplace transform of f
h	thickness of the skin
J	transdermal flux at the skin/blood interface
$\bar{J}$	Laplace transform of J
k_{12}	rate constant for drug transfer from the central to the peripheral compartment
k_{21}	rate constant for drug transfer from the peripheral to the central compartment
k_e	elimination rate constant
P	function defined in Eq. (27)
P_1	function defined in Eq. (41)
P_2	function defined in Eq. (42)
Q	function defined in Eq. (28)
s	Laplace transform variable
t	time
$t_{c,1}$	time constant of a one-compartment model; the flux (J) and the concentration (C_p) are the input and output variables, respectively
$t_{c,2}$	time constant of the central compartment of a two-compartment model; the flux (J) and the concentration (C_p) are the input and output variables, respectively
t_{eff}	effective time constant
$t_{eff,p1}$	effective time constant of a one-compartment model; the surface concentration (C_s) and the plasma drug concentration (C_p) are the input and output variables, respectively
$t_{eff,p2}$	effective time constant of the central compartment of a one-compartment model; the surface concentration (C_s) and the plasma drug concentration (C_1) are the input and output variables, respectively
$t_{eff,sk}$	effective time constant of the skin; the surface concentration (C_s) and the flux (J) are the input and output variables, respectively
x	distance variable
V	apparent volume of distribution of a one-compartment model
V_1	volume of central compartment of a two-compartment model
V_2	volume of peripheral compartment of a two-compartment model

Greek letters

ν	iontophoretic model parameter
Ω	probability density function defined by Eq. (11)
λ_n	eigen-value defined by Eq. (22)

iontophoresis [10]. As noted in [9], a steady-state flux is not achieved so quickly in some cases. Nevertheless, in spite of their practicality and superiority, conclusions based on a compartmental analysis may not have general applicability. This observation was shared by Nugroho et al. (2002), who agreed that further experiments were needed before extrapolating, to other compounds, the results from the R-apomorphine study. A mathematical representation, based on first principles, seems better suited for modeling transport by iontophoresis. We are able to translate the results to a number of medications because the equations are functions of a compound's physical properties.

This contribution puts forward a novel modeling approach, based on transport equations, for predicting *in-vivo* data from *in-vitro* experiments. Conditions under which the constant flux approximation is valid for estimating plasma drug concentration will also be discussed. In the case of one- or two-compartment models, the objective of the new procedure is to show that the ratio of two time constants can be applied to predict when the steady-state flux is adequate for estimating *in-vivo* iontophoretic data. Equations for calculating plasma drug concentrations are proposed. New correlations are also offered for predicting *in-vivo* data when the steady-state flux assumption does not hold. Only the pharmacokinetic parameters of the drug and model parameters, obtained from *in-vitro* experiments, are necessary in the suggested framework. The paper will introduce the analysis in terms of time constants for medications in the skin and the blood compartment. Contrary to other methods, the suggested technique provides analytical expressions for the time constants and provides expressions for the plasma drug concentration even when it takes a long time to reach a steady-state flux.

2. Theory

2.1. Mathematical modeling

2.1.1. Single skin layer (stratum corneum)

The transport equation for iontophoretic delivery is [11]

$$\frac{\partial C}{\partial t} = D\frac{\partial^2 C}{\partial x^2} - \frac{\nu D}{h}\frac{\partial C}{\partial x} \tag{1}$$

where C is the drug concentration in the skin; ν is a parameter which depends on the charge number on the drug and the potential difference across the skin; h is the skin thickness; D is the drug diffusivity in the skin. Eq. (1) assumes a small convective flow. The model neglects tissue binding and metabolic processes in the skin. Initially, the skin is free of the drug:

$$C(x, 0) = 0 \tag{2}$$

The boundary conditions are

$$C(0, t) = C_s \tag{3}$$

$$C(h, t) = 0 \tag{4}$$

with C_s representing the surface concentration at the skin-vehicle interface. The concentration C_s is constant because the drug loading dose is assumed well above the saturated drug concentration in the patch. Eq. (4) states that the drug is instantly removed beneath the stratum corneum and into the systemic circulation so that its concentration remains low compared to the saturated drug concentration.

The delivery rate is given by

$$J(t) = -D\frac{\partial C}{\partial x}\bigg|_{x=h} \tag{5}$$

A closed-form solution for the cumulative amount of drug released for the system determined by Eqs. (1)–(4) is provided in [11] and [12].

2.1.2. One-compartment model for drug elimination and time constant

A mass balance around the single compartment yields

$$V\frac{dC_p}{dt} = J(t)A - k_e C_p V \tag{6}$$

with the following initial condition:

$$C_p(0) = 0 \tag{7}$$

where V represents the apparent volume of distribution, A is the surface area of the transdermal patch, k_e is the elimination rate constant and C_p is the plasma drug concentration. The time constant ($t_{c,1}$) is determined by first writing Eq. (6) in standard form

$$\frac{1}{k_e}\frac{dC_p}{dt} + C_p = \frac{A}{k_e}J(t) \tag{8}$$

which gives

$$t_{c,1} = \frac{1}{k_e} \tag{9}$$

In the context of process dynamics and control, C_p and J represents output and input variables, respectively. Note that an effective time constant defined as [13]

$$t_{eff} = \int_0^\infty t\Omega(t)dt \tag{10}$$

where $\Omega(t)$ is represented by

$$\Omega(t) = \frac{(f(\infty) - f(t))}{\int_0^\infty (f(\infty) - f(t))dt} \tag{11}$$

gives the result shown in Eq. (9). The function $f(t)$ is monotonic. It can be shown that t_{eff} can be written in the form [13]

$$t_{eff} = \frac{\lim\limits_{s\to 0}\left(\frac{f(\infty)}{s^2} + \frac{d\bar{F}(s)}{ds}\right)}{\lim\limits_{s\to 0}\left(\frac{f(\infty)}{s} - \bar{F}(s)\right)} \tag{12}$$

where $\bar{F}(s)$ is the Laplace transform of $f(t)$. The advantage of applying Eq. (10) or (12) is that researchers will be able to assess the dynamics of high-order systems, including 2nd order and diffusive processes, by using a single parameter. This performance criterion is a measure of the time it takes to reach a steady-state value, just like the time constant of a first-order system.

2.1.3. Two-compartment model for drug elimination and time constant

Mass balances around the central and peripheral compartments give [14]

$$V_1\frac{dC_1}{dt} = J(t)A + k_{21}C_2V_2 - (k_{12} + k_e)C_1V_1 \tag{13}$$

and

$$V_2\frac{dC_2}{dt} = k_{12}C_1V_1 - k_{21}C_2V_2 \tag{14}$$

respectively. The initial conditions are

$$C_1(0) = 0 \tag{15}$$

and

$$C_2(0) = 0 \tag{16}$$

In the above equations, V_1 and V_2 represent the apparent volumes of distribution in the central and peripheral compartments, respectively; C_1 and C_2 are the drug concentrations in the central and peripheral compartments; k_{12} is the rate constant for drug transfer from the central to the peripheral compartment and k_{21} is the rate constant for drug transfer from the peripheral to the central compartment. An effective time constant for $C_1(t)$ is calculated:

$$t_{c,2} = \frac{k_{12}^2 + 2k_{12}k_{21} + k_{21}^2 + k_{12}k_e}{k_{21}^2k_e + k_{12}k_{21}k_e} \tag{17}$$

In this case, the output is $C_1(t)$. Note that when $k_{12} = 0$ (i.e., a one-compartment model), Eq. (17) reduces to Eq. (9). We are able to conduct a similar analysis for compartment 2. However, the focus is the plasma drug concentration because it is most commonly measured in clinical studies.

2.2. Dynamics of transdermal drug transport, distribution and elimination

2.2.1. Transport dynamics in the skin layer

The Laplace transform of Eq. (1) gives

$$s\bar{C}(x,s) = D\frac{d^2\bar{C}(x,s)}{dx^2} - \frac{\nu D}{h}\frac{d\bar{C}(x,s)}{dx} \tag{18}$$

after applying the initial condition (2), where $\bar{C}(x,s)$ denotes the Laplace transform of $C(x,t)$. The solution of Eq. (18), with the Laplace transforms of boundary conditions (3) and (4), leads to

$$\bar{C}(x,s) = \frac{C_s e^{\frac{x\nu}{2h}}}{s}\operatorname{csch}\left(\frac{1}{2}h\sqrt{\frac{4s}{D} + \frac{\nu^2}{h^2}}\right)\sinh\left(\frac{1}{2}(h-x)\sqrt{\frac{4s}{D} + \frac{\nu^2}{h^2}}\right) \tag{19}$$

Eqs. (19) and (5) yield

$$\bar{J}(s) = \frac{C_sD}{2s}e^{\nu/2}\sqrt{\frac{4s}{D} + \frac{\nu^2}{h^2}}\operatorname{csch}\left(\frac{1}{2}h\sqrt{\frac{4s}{D} + \frac{\nu^2}{h^2}}\right) \tag{20}$$

The inverse Laplace transform of Eq. (20) is computed using the Bromwich integral and the residue theorem:

$$J(t) = \frac{C_sDe^\nu\nu}{(e^\nu - 1)h} + \sum_{n=1}^{\infty}\left(\frac{8(-1)^nC_sDe^{\nu/2}n^2\pi^2}{h(4n^2\pi^2 + \nu^2)}\right)e^{-\lambda_n t} \tag{21}$$

where

$$\lambda_n = \frac{4Dn^2\pi^2 + D\nu^2}{4h^2} \tag{22}$$

and the steady-state flux takes the form

$$J(\infty) = \frac{C_sDe^\nu\nu}{(e^\nu - 1)h} \tag{23}$$

Eq. (21) was published in [11]. The effective time constant ($t_{eff,sk}$), used for estimating the time to establish a steady-state flux in the skin layer, was previously derived [15]:

$$t_{eff,sk} = \frac{h^2\left(3\nu^2 - 2sinh(\nu)\nu + \left(\nu^2 - 4\right)cosh(\nu) + 4\right)}{2D\nu^2(2 - 2cosh(\nu) + \nu sinh(\nu))} \tag{24}$$

2.2.2. Plasma drug concentration assuming a one-compartment model for drug elimination

The Laplace transform of Eq. (6) gives

$$\bar{C}_p(s) = \frac{A\bar{J}(s)}{(k_e + s)V} \tag{25}$$

or

$$\bar{C}_p(s) = \frac{AC_sDe^{\nu/2}\sqrt{\frac{4s}{D}+\frac{\nu^2}{h^2}}}{2sV(k_e+s)\sinh\left(\frac{1}{2}h\sqrt{\frac{4s}{D}+\frac{\nu^2}{h^2}}\right)} \tag{26}$$

After defining the following functions:

$$P(s) = AC_sDe^{\nu/2}\sqrt{\frac{4s}{D}+\frac{\nu^2}{h^2}} \tag{27}$$

and

$$Q(s) = 2sV(k_e+s)\sinh\left(\frac{1}{2}h\sqrt{\frac{4s}{D}+\frac{\nu^2}{h^2}}\right) \tag{28}$$

the inverse Laplace transform of Eq. (25) is computed using the Bromwich integral and the residue theorem:

$$C_p(t) = \frac{AC_se^{\nu}D\nu}{h(e^{\nu}-1)Vk_e} + \frac{P(-k_e)}{\frac{dQ(s)}{ds}\Big|_{s=-k_e}}e^{-k_et} + \sum_{n=1}^{\infty}\frac{P(s_n)}{\frac{dQ(s)}{ds}\Big|_{s=s_n}}e^{s_nt} \tag{29}$$

with

$$s_n = -\frac{4Dn^2\pi^2+D\nu^2}{4h^2} \tag{30}$$

or

$$C_p(t) = \frac{AC_se^{\nu}D\nu}{h(e^{\nu}-1)Vk_e} - \frac{1}{2}\frac{AC_se^{\frac{\nu}{2}-tk_e}\sqrt{D(D\nu^2-4h^2k_e)}}{h\sinh\left(\frac{1}{2}\frac{\sqrt{D(D\nu^2-4h^2k_e)}}{D}\right)Vk_e} - \sum_{n=1}^{\infty}\frac{32AC_s\pi^2Dn^2h}{V(4n^2\pi^2+\nu^2)(-1)^n(4n^2\pi^2D+D\nu^2-4h^2k_e)} \times e^{-\frac{4Dtn^2\pi^2+Dt\nu^2-2\nu h^2}{4h^2}} \tag{31}$$

To our knowledge, Eq. (31) has not been derived before. The steady-state plasma concentration is

$$C_p(\infty) = \frac{AC_se^{\nu}D\nu}{h(e^{\nu}-1)Vk_e} \tag{32}$$

If we consider the surface concentration C_s as the input and $C_p(t)$ as the output, the effective time constant to reach $C_p(\infty)$ is

$$t_{eff.p1} = -\frac{4Dh^2k_e\nu^2 - 2D^2\nu^4 + h^4{k_e}^2(4+\nu^2) + 2h^2k_e\nu(h^2k_e - D\nu^2)\coth\left(\frac{\nu}{2}\right) - 2h^4{k_e}^2\nu^2\coth\left(\frac{\nu}{2}\right)^2}{2Dk_e\nu^2\left(-2h^2k_e + D\nu^2 + h^2k_e\nu\coth\left(\frac{\nu}{2}\right)\right)} \tag{33}$$

Eq. (33) is the product of two process units: the skin and the blood compartment.

When $t_{c,1} \gg t_{eff.sk}$ (i.e., the skin is not rate-limiting), it is appropriate to write $J(t) = J(\infty)$. Therefore, the solution to Eq. (8) reduces to

$$C_p(t) = \frac{J(\infty)A}{k_eV}(1-e^{-k_et}) \tag{34}$$

Further examination reveals that the steady-state $C_p(\infty)$, deduced from Eq. (31) and given by Eq. (32), can also be derived from Eq. (34). Following transdermal iontophoresis, Eq. (34) is appropriate for predicting *in-vivo* pharmacokinetics from *in-vitro* experiments only when $t_{c,1} \gg t_{eff.sk}$. In all other cases, Eq. (31) should be employed and $t_{eff.p1}$ is a better indicator of the time elapsed before reaching $C_p(\infty)$ than $t_{c,1}$ (or k_e). Note that $t_{eff.sk}$, defined by Eq. (24), can be computed from *in-vitro* Franz diffusion experiments using analyses provided in [11,12,16].

2.2.3. Plasma drug concentration assuming a two-compartment model for drug elimination

It can be shown that the Laplace transforms of $C_1(t)$ and $C_2(t)$ are

$$\bar{C}_1(s) = \frac{(k_{21}+s)A\bar{J}(s)}{(k_{21}k_e+k_{12}s+k_{21}s+k_es+s^2)V_1} \tag{35}$$

and

$$\bar{C}_2(s) = \frac{k_{12}A\bar{J}(s)}{(k_{21}k_e+k_{12}s+k_{21}s+k_es+s^2)V_2} \tag{36}$$

respectively. Substituting $\bar{J}(s)$, defined by Eq. (20), in Eqs. (35) and (36), we find

$$\bar{C}_1(s) = \frac{\frac{AC_sD}{V_1}(k_{21}+s)e^{\nu/2}\sqrt{\frac{4s}{D}+\frac{\nu^2}{h^2}}}{2s(k_{21}k_e+k_{12}s+k_{21}s+k_es+s^2)\sinh\left(\frac{1}{2}h\sqrt{\frac{4s}{D}+\frac{\nu^2}{h^2}}\right)} \tag{37}$$

and

$$\bar{C}_2(s) = \frac{\frac{AC_sD}{V_2}k_{12}e^{\nu/2}\sqrt{\frac{4s}{D}+\frac{\nu^2}{h^2}}}{2s(k_{21}k_e+k_{12}s+k_{21}s+k_es+s^2)\sinh\left(\frac{1}{2}h\sqrt{\frac{4s}{D}+\frac{\nu^2}{h^2}}\right)} \tag{38}$$

The poles of Eq. (38) are

$$s_{01} = -\frac{1}{2}k_{21} - \frac{1}{2}k_{12} - \frac{1}{2}k_e - \frac{1}{2}\sqrt{{k_{12}}^2+2k_{21}k_{12}+2k_{12}k_e+{k_{21}}^2-2k_ek_{21}+{k_e}^2} \tag{39}$$

$$s_{02} = -\frac{1}{2}k_{21} - \frac{1}{2}k_{12} - \frac{1}{2}k_e + \frac{1}{2}\sqrt{{k_{12}}^2+2k_{21}k_{12}+2k_{12}k_e+{k_{21}}^2-2k_ek_{21}+{k_e}^2} \tag{40}$$

and s_n is defined by Eq. (30). Setting

$$P_1(s) = \frac{AC_sD}{V_1}(k_{21}+s)e^{\nu/2}\sqrt{\frac{4s}{D}+\frac{\nu^2}{h^2}} \tag{41}$$

$$P_2(s) = \frac{AC_sD}{V_2}k_{12}e^{\nu/2}\sqrt{\frac{4s}{D}+\frac{\nu^2}{h^2}} \tag{42}$$

and

$$Q(s) = 2s\left(k_{21}k_e+k_{12}s+k_{21}s+k_es+s^2\right)\sinh\left(\frac{1}{2}h\sqrt{\frac{4s}{D}+\frac{\nu^2}{h^2}}\right) \tag{43}$$

the concentrations in the two compartments become

$$C_1(t) = \frac{AC_se^{\nu}D\nu}{h(e^{\nu}-1)V_1k_e} + \sum_{i=1}^{2}\frac{P_1(s_{0i})}{\frac{dQ(s)}{ds}\Big|_{s=s_{0i}}}e^{s_{0i}t} + \sum_{n=1}^{\infty}\frac{P_1(s_n)}{\frac{dQ(s)}{ds}\Big|_{s=s_n}}e^{s_nt} \tag{44}$$

$$C_2(t) = \frac{AC_s e^{\nu} D\nu k_{12}}{h(e^{\nu}-1)V_2 k_e k_{21}} + \sum_{i=1}^{2} \frac{P_2(s_{0i})}{\left.\frac{dQ(s)}{ds}\right|_{s=s_{0i}}} e^{s_{0i}t} + \sum_{n=1}^{\infty} \frac{P_2(s_n)}{\left.\frac{dQ(s)}{ds}\right|_{s=s_n}} e^{s_n t} \quad (45)$$

Therefore, the steady-state plasma concentration $C_1(\infty)$ is given by

$$C_1(\infty) = \frac{AC_s e^{\nu} D\nu}{h(e^{\nu}-1)V_1 k_e} \quad (46)$$

and the associated time constant is

$$t_{eff,p2} = \frac{\left[\begin{array}{l} D^2(e^{\nu}-1)^2\nu^4\left(k_{12}k_e + (k_{12}+k_{21})^2\right) + Dh^2k_{21}(k_{12}+k_{21})(e^{\nu}-1)\nu^2(e^{\nu}(\nu-2)+\nu+2)k_e \\ \quad + h^4k_{21}^2e^{\nu}k_e^2\left(3\nu^2 + \left(\nu^2-4\right)cosh(\nu) - 2\nu sinh(\nu) + 4\right) \end{array}\right]}{Dk_{21}(e^{\nu}-1)\nu^2k_e\left(D(k_{12}+k_{21})(e^{\nu}-1)\nu^2 + h^2k_{21}(e^{\nu}(\nu-2)+\nu+2)k_e\right)} \quad (47)$$

When $t_{c,2} \gg t_{eff,sk}$, we have $J(t) = J(\infty)$ and Eq. (35) becomes

$$\bar{C}_1(s) = \frac{(k_{21}+s)AJ(\infty)}{s(k_{21}k_e + k_{12}s + k_{21}s + k_e s + s^2)V_1} \quad (48)$$

which gives

$$C_1(t) = -\frac{J(\infty)Ae^{-\frac{1}{2}t(k_e+k_{12}+k_{21}+\phi)}}{2V_1k_e\phi}\left(-2\phi e^{\frac{1}{2}t(k_e+k_{12}+k_{21}+\phi)} - k_e e^{t\phi} + k_e + k_{12}e^{t\phi} + k_{21}e^{t\phi} - k_{12} - k_{21} + \phi e^{t\phi} + \phi\right) \quad (49)$$

after inverting Eq. (48). The parameter ϕ is

$$\phi = \sqrt{(k_e+k_{12}+k_{21})^2 - 4k_{21}k_e} \quad (50)$$

The newly developed expressions (44), (47) and (49) can be utilized to predict the dynamics of plasma drug concentration as a function of the electric field and the drug's kinetic and physicochemical characteristics. Following an analysis similar to the one offered in Section 1.2.2, Eq. (49) is suitable for estimating *in-vivo* pharmacokinetics from *in-vitro* data only when $t_{c,2} \gg t_{eff,sk}$. In all other cases, Eq. (44) should be used. The parameter $t_{eff,p2}$ is the appropriate time constant for these systems.

3. Methods

For both, 1- and 2-compartmental pharmacokinetics, we first compared the predictions of the approximation and the new mechanism-based method using two examples. Simulations for transdermal drug administration were performed based on PK parameters from *i.v.* drug administration and transport properties assessed *in-vitro* (known or assumed). Mathematica 10.0.1 (Wolfram Research, Inc., Champaign, IL) was employed for the simulations and for fitting plasma drug concentrations to a specified model with the least-squares minimization routine *NonLinearModelFit*. The digitizing software FindGraph 2.59 (UNIPHIZ Lab) was used to extract the data values.

3.1. One-compartment model

The constant flux approximation and the new approach were tested through simulations and published experimental data. For a one-compartment model, the tricyclic antidepressant amitriptyline (HCl) was selected. The mean pharmacokinetic constants, obtained after administration of a single dose of amitriptyline, are [17]: $V = 19(\pm 4.2)$l/kg and $k_e = 0.033\,h^{-1}$ (i.e., average half-life of 21 h ($\pm$ 4.8 h) (Table 1). *In-vitro* Franz diffusion cell experiments were performed and analyzed to study iontophoretic delivery of the drug across human skin samples [16]. The model parameters ($\pm$ standard error) are: $\nu = 1.36$ ($\pm$ 6.98), $D = 1.79 \times 10^{-4}(\pm 2.06 \times 10^{-5})cm^2/h$, $A = 0.634cm^2$, $h = 500\,\mu m$ and $C_s = 7933.17(\pm 21498.10)\,\mu g/ml$. The donor cell concentration was 0.032 M and the current density was maintained at 0.2 mA/cm^2 for 8 h. Simulations were conducted to assess the impact on $C_p(t)$ and $t_{eff,p}$ of changes in the elimination rate constant, from the reference k_e value. The normalized integral of squared error (ISE): $\int_0^{t_f}\left(\frac{Cp_{trans}(t)-Cp_{stead}(t)}{Cp_{trans}(\infty)}\right)^2 dt$ and the ratio of the effective time constant in the compartment ($t_{c,1}$) to that in the skin layer $t_{eff,sk}$ were also calculated as a function of k_e. The function $Cp_{trans}(t)$ was $C_p(t)$ computed from Eq. (31) while $Cp_{stead}(t)$ approximated $Cp(t)$ only when the steady-state flux was included in the computation (Eq. (34)). The constant t_f was set to a sufficiently large value to estimate the upper limit of integration ∞.

The applicability of the IVIVC was evaluated using experimental plasma concentration of the growth-hormone releasing factor (GRF) administered by transdermal iontophoresis into hairless guinea pigs for a duration of 5 h [9]. The total thickness of hairless guinea pig skin was $h = 1.5$ mm (range: 1 to 2 mm) [18] and the patch area was $A = 5cm^2$ [9]. The mean pharmacokinetic parameters of GRF were [19] $V = 8.861(\pm 0.530)$l and $k_e = 1.782\,h^{-1}$ (i.e., average half-life of 0.389 hours ($\pm$ 0.332 h) (Table 1).

3.2. Two-compartment model

Simulations were performed to test the approach outlined in Section 2.2.3. We considered a two-compartment model for disposition of dexamethasone sodium-m-sulfobenzoate (DMSB) after intravenous administration to 10 fasted volunteers (n = 10) [20]. The mean pharmacokinetic parameters derived from the single-dose investigation were: $V_1 = 38133.8$ ml(plasma compartment), $V_2 = 76518.7$ml(tissue compartment), $k_{12} = 2.945\,h^{-1}$, $k_{21} = 1.468\,h^{-1}$ and $k_e = 0.474\,h^{-1}$ (Table 1). The iontophoretic parameters were computed from data published in [12]: $\nu = 0.055(\pm 0.10)$, $D = 5.69 \times 10^{-5}(\pm 2.11 \times 10^{-6})cm^2/h$, $A = 0.64cm^2$, $h = 0.035cm$ and $C_s = 3718.62(\pm 5.6 \times 10^{-5})\,\mu g/ml$. The standard errors were calculated using the inverse of the square root of the diagonal elements of the Fisher information matrix. A current density of 0.30 mA/cm^2 was applied for 6 hours. The simulation study is intended to address the

Table 1
Mean pharmacokinetic parameters for one-compartment and two-compartment models.

		One-compartment model	
		Amitriptyline (HCl)	GRF
V	ml	1.33E + 06	8.86
k_e	h^{-1}	0.033	1.78
$t_{c,1}$	h	30.3	0.56
		Two-compartment model	
		DMSB	Naloxone
V_1	ml	38133.8	891.7
V_2	ml	76518.7	1452.0
k_{12}	h^{-1}	2.95	8.89
k_{21}	h^{-1}	1.47	5.46
k_e	h^{-1}	0.47	5.24
$t_{c,2}$	h	6.8	0.6

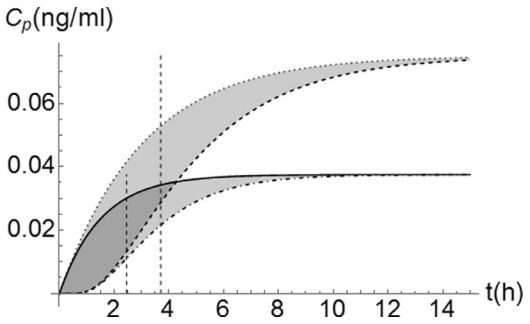

Fig. 1. Plasma concentration of amitriptyline (HCl) C_p when a one-compartment model is applied. For the simulations, the elimination rate constants are set to 10 × k_e and 20 × k_e. Predictions based on the steady-state (dotted line: …) and transient fluxes (dashed line: —) are shown for 10 × k_e. The curves (dot-dashed line: .-.-.-.-) and (solid line: –) represent concentrations calculated from the equilibrium and dynamic fluxes, respectively, for 20 × k_e. The time constants $t_{eff,p1}$, indicated by vertical lines, are 3.70 h (10 × k_e) and 2.45 h (20 × k_e).

influence on $C_p(t)$ and $t_{eff,p2}$ of changes in the elimination rate constant, from its reference value. The ratio $t_{c,2}/t_{eff,sk}$ was computed as a function of ISE: $\int_0^{t_f}\left(\frac{Cp_{trans}(t)-Cp_{stead}(t)}{Cp_{trans}(\infty)}\right)^2 dt$ where $Cp_{trans}(t)$ represents $C_p(t)$ computed from Eq. (44) and $Cp_{stead}(t)$ stands for $Cp(t)$ calculated from Eq. (49).

Experimental plasma concentrations of naloxone, an opioid antagonist, after transdermal iontophoresis in conscious rats [21] were selected to test the procedure (current application: 24 h). The thickness of the dermal layer is $h = 0.075$cm and the *in-vivo* patch area available for diffusion was $A = 1.13\text{cm}^2$ [21]. The mean pharmacokinetic parameters of the drug were drawn from the literature (n = 3) [21]: $V_1 = 891.7$ ml(plasma compartment), $V_2 = 1452.0$ml(tissue compartment), $k_{12} = 8.89\,\text{h}^{-1}$, $k_{21} = 5.46\,\text{h}^{-1}$ and $k_e = 5.24\,\text{h}^{-1}$ (Table 1).

4. Results and discussions

4.1. One-compartment model

For computations involving amitriptyline (HCl) as a reference and a one-compartment model, the drug elimination rate constants are set to $0.33\,\text{h}^{-1}$ and $0.66\,\text{h}^{-1}$ (Fig. 1). Predictions based on the steady-state (dotted line: …) and transient fluxes (dashed line: —) are shown for $0.33\,\text{h}^{-1}$. The curves, dot-dashed line: .-.-.-.- and solid line: –, represent concentrations calculated from the equilibrium and dynamic fluxes, respectively, for $k_e = 0.66\,\text{h}^{-1}$. The time constants $t_{eff,p1}$, indicated by vertical lines, are 3.70 h ($0.33\,\text{h}^{-1}$) and 2.45 h ($0.66\,\text{h}^{-1}$). As k_e increases, the plasma drug concentration and the time required to reach the plateau decrease. In addition, the ratio $t_{c,1}/t_{eff,sk}$ is 1.93 and 0.96 for $k_e = 0.33\,\text{h}^{-1}$ and $k_e = 0.66\,\text{h}^{-1}$, respectively. Therefore, the time constants are of the same order of magnitude which explains the large discrepancies between predictions based on the equilibrium and transient fluxes. This point is further illustrated in Fig. 2 where the error $ISE = \int_0^{t_f}\left(\frac{Cp_{trans}(t)-Cp_{stead}(t)}{Cp_{trans}(\infty)}\right)^2 dt$ and $t_{c,1}/t_{eff,sk}$ are shown in terms of k_e. As $t_{c,1}/t_{eff,sk}$ increases, $Cp_{stead}(t)$ approaches $Cp_{trans}(t)$.

GRF delivery data from guinea pigs were used to test the one-compartment model. Fig. 3 displays experimental plasma concentration of GRF after transdermal iontophoresis in hairless guinea pigs (•). The estimated parameters of the transdermal iontophoretic model are (*NonLinearModelFit*, Mathematica): $\nu = 0.379(\pm 0.83)$, $D = 6.84 \times 10^{-3}(\pm 0.002)\text{cm}^2/\text{h}$ and $C_s = 11.9\,\mu\text{g/ml}$. The high standard deviation (SD) in ν means that its estimated value is less accurate than those of D and C_s. This may be due to insufficient data in the transient regime. A negligible SD is observed for C_s. Solid lines (–) represent the fitted C_p profiles based on the transient flux. Dot-dashed lines (.-.-.-.-) show the predicted plasma GRF concentration calculated using the steady-state flux of $J(\infty) = 677.4\text{ngcm}^{-2}\,\text{h}^{-1}$ listed in [9]. In this case, the ratio $t_{c,1}/t_{eff,sk}$ is 1.47 and the plasma drug level should be estimated by $Cp_{trans}(t)$.

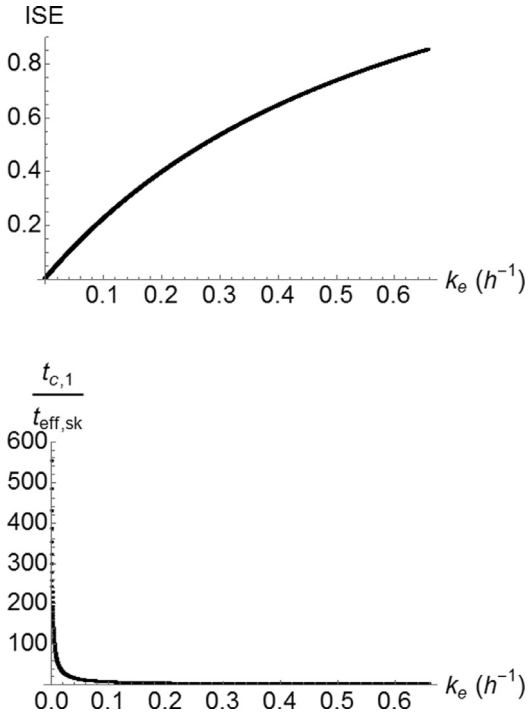

Fig. 2. Effects of the elimination rate constant on ISE (normalized integral of squared error) and $t_{c,1}/t_{eff,sk}$, i.e., the ratio of the effective time constant in the single compartment ($t_{c,1}$) to that in the skin layer $t_{eff,sk}$. The elimination rate constant is varied from 0.01 × k_e to 20 × k_e for the simulations. ISE stands is defined by $\int_0^{t_f}\left(\frac{Cp_{trans}(t)-Cp_{stead}(t)}{Cp_{trans}(\infty)}\right)^2 dt$. $Cp_{trans}(t)$ is the estimated plasma drug concentration when the transient flux is used; $Cp_{stead}(t)$ approximates $Cp(t)$ when only the steady-state flux is included in the computation. The upper limit of integration t_f is set to 10^3 h.

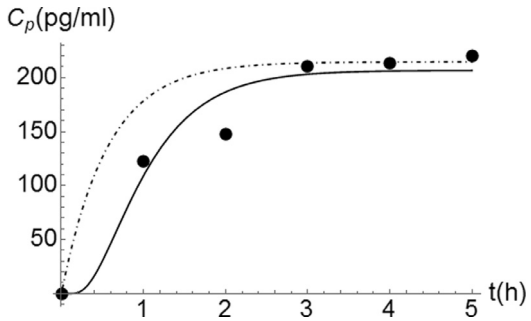

Fig. 3. Plasma concentration of the growth-hormone releasing factor (GRF) after transdermal iontophoresis in hairless guinea pigs. The solid circles (•) refer to experimental data. Dot-dashed lines (.-.-.-.-) show the predicted plasma GRF concentration based on a steady-state flux of $J(\infty) = 677.4\text{ngcm}^{-2}\,\text{h}^{-1}$. Solid lines (–) represent the fitted C_p profiles based on the transient flux.

4.2. Two-compartment model

To conduct the simulation study, two elimination rate constants are selected: $0.94\,\text{h}^{-1}$ and $4.7\,\text{h}^{-1}$. The remaining model parameters correspond to the release of DMSB following transdermal iontophoretic delivery (see Section 3.2). Plasma drug concentrations calculated using the steady-state (dotted line: …) and transient fluxes (dashed line: —) are displayed for $0.94\,\text{h}^{-1}$(Fig. 4). The dot-dashed (.-.-.-.-) and solid lines (–) represent predictions from the equilibrium and transient fluxes, respectively, for $4.7\,\text{h}^{-1}$. The time constants $t_{eff,p2}$, specified by vertical lines, are approximated as 4.74 h

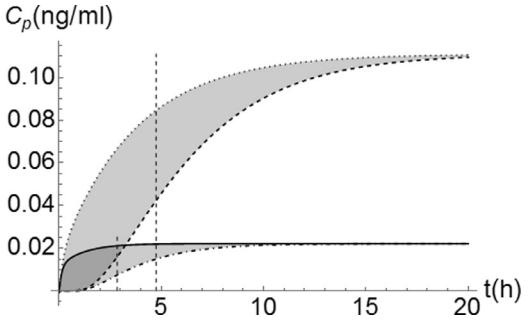

Fig. 4. Plasma concentration of dexamethasone sodium-m-sulfobenzoate (DMSB) C_p when a two-compartment model is applied. For the simulations, the elimination rate constants are set to $2 \times k_e$ and $10 \times k_e$. Predictions based on the steady-state (dotted line: ...) and transient fluxes (dashed line: —) are shown for $2 \times k_e$. The curves (dot-dashed line: .-.-.-.-) and (solid line: –) represent concentrations calculated from the equilibrium and dynamic fluxes, respectively, for $10 \times k_e$. The time constants $t_{eff,p2}$, specified by vertical lines, are 4.74 h ($2 \times k_e$) and 2.84 h ($10 \times k_e$).

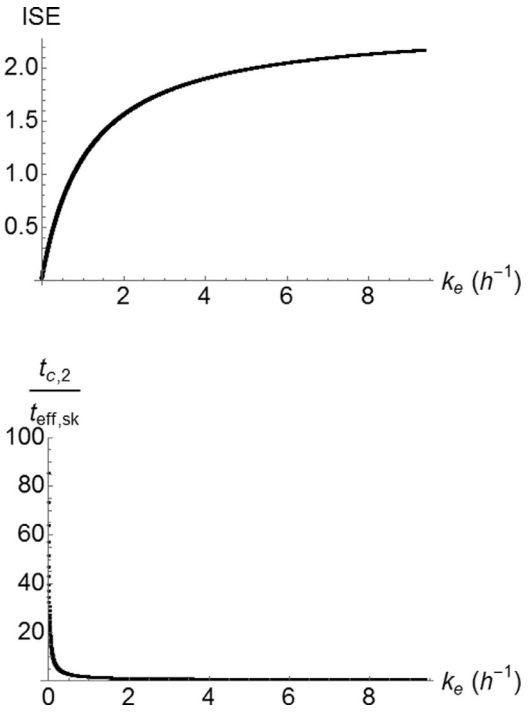

Fig. 5. Effects of the elimination rate constant on ISE (normalized integral of squared error) and $t_{c,2}/t_{eff,sk}$, i.e., the ratio of the effective time in the central compartment ($t_{c,2}$) to that in the skin layer $t_{eff,sk}$. The elimination rate constant is varied from $0.01 \times k_e$ to $20 \times k_e$ for the simulations. ISE stands for the normalized integral of squared error and is defined by $\int_0^{t_f} \left(\frac{Cp_{trans}(t) - Cp_{stead}(t)}{Cp_{trans}(\infty)}\right)^2 dt$. $Cp_{trans}(t)$ is the estimated plasma drug concentration when the transient flux is used; $Cp_{stead}(t)$ approximates $Cp(t)$ when only the steady-state flux is included in the calculations. The upper limit of integration t_f is set to 10^3 h.

($0.94\,h^{-1}$) and 2.84 h ($4.7\,h^{-1}$). As k_e increases, the plasma drug level and the time elapsed, before reaching a steady-state value, is reduced. The fraction $t_{c,2}/t_{eff,sk}$ is 1.45 and 0.44 when $k_e = 0.94\,h^{-1}$ and $k_e = 4.7\,h^{-1}$, respectively. These data reveal no order-of-magnitude differences in the time constants associated with the skin and the central compartment. However, a more reliable prediction of the plasma drug concentration is expected for $k_e = 0.94\,h^{-1}$ when $J(\infty)$ is used. This observation is corroborated by Fig. 5 which shows a decline in *ISE* as k_e decreases leading to an increase in $t_{c,2}/t_{eff,sk}$.

Fig. 6 shows the plasma concentration of naloxone (•) after transdermal iontophoresis in rats [21]. The fitted iontophoretic parameters are (*NonLinearModelFit, Mathematica*): $\nu = 1.92(\pm 1.42)$, $D = 2.73 \times 10^{-3}(\pm 1.30 \times 10^{-3})\,cm^2/h$ and $C_s = 1.56 \times 10^6(\pm 3.13 \times 10^{-6})$ ng/ml. The dot-dashed lines (.-.-.-.-) show $Cp_{stead}(t)$ when the steady-state

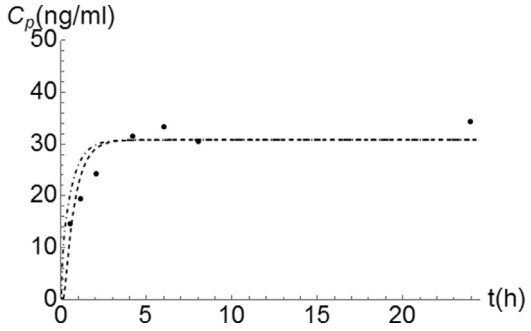

Fig. 6. Plasma concentration of naloxone after transdermal iontophoresis in rats. The solid circles (•) represent experimental data. Dot-dashed lines (.-.-.-.-) show the predicted plasma naloxone concentration based on the steady-state flux of $J(\infty) = 127.6\,\mu g cm^{-2}\,h^{-1}$. Solid lines (–) show the fitted C_p profiles based on the transient flux.

flux of $J(\infty) = 127.6\,\mu g cm^{-2}\,h^{-1}$ is used while the solid lines (–) represent $Cp_{trans}(t)$. The time constant ratio $t_{c,2}/t_{eff,sk}$ is 2.75, which means that $Cp_{stead}(t)$ is, not surprisingly, a reasonable representation of $C_p(t)$.

Compared to current methods of predicting plasma drug concentration based on steady-state transdermal flux, the proposed methodology assesses the accuracy of such estimations, as well. As noted in the studies outlined above, the technique is relevant to one- and two-compartment models describing drug elimination in the body. Equations are also provided for cases where steady-state approximations are inadequate ($t_{c,1}/t_{eff,sk} \leq 1$ or $t_{c,2}/t_{eff,sk} \leq 1$). This tool offers the possibility to develop reliable IVIVCs for devices designed for transdermal iontophoresis. The approach has the potential to reduce the number of *in-vivo* experiments and to predict the performance of new devices more accurately based on *in-vitro* data. Because the procedure considers drug transport through the skin and subsequent elimination as two processes in series, the application can be extended to other systems. For example, physiologically-based pharmacokinetic (PBPK) models can be applied in lieu of the one- or two-compartment kinetics. The ratio of the time constants would determine which process unit exhibits slow or fast dynamics. The efficiency of the method is expected to be affected by individual variability, measurement error and the accuracy of the pharmacokinetic estimates. Simulation shows the plasma concentration profiles are sensitive to C_s, D and ν in the cases of one- and two-compartment models (results not shown). Note that the models proposed do not consider factors that may affect the bioavailability of therapeutics, such as drug inactivation caused by skin metabolism and interaction between the drug and penetration enhancers.

This approach is based on the fact that, for two processes in series, the slower unit (i.e., longer time constant) governs the overall dynamic behavior of the system. The present work considers iontophoretic transport through the skin followed by body distribution and elimination as two such processes (I and II, respectively). Because it is possible to compute effective time constants for both systems, we use the ratio (II:I) as a criterion to determine which process is dominant. If the ratio is small, it takes the drug a relatively long time to reach the skin/blood interface. Consequently, ignoring the dynamics of drug transport through skin and assuming a steady-state flux would yield significant errors. The approximation is valid when the ratio is large. When the ratio is approximately one, both processes contribute to the observed transient behavior.

The computation of an effective time constant clarifies observations made in the laboratory. An infusion model that uses a steady-state input flux from *in-vitro* data may be the simplest method to predict *in-vivo* plasma concentrations. However, the error may be significant, especially at early time-points, if the steady state is not reached rapidly. This work suggests an analysis based on the ratio of

the time constants to gauge the accuracy of the IVIVC. In addition, equations are provided to calculate the time constants and estimate the plasma blood concentrations even when the skin is rate-limiting.

Note that, in clinical settings, there is a relationship between the steady-state flux and plasma concentration. The current intensity and drug concentration in the patch can influence the steady-state flux up to a certain threshold. *In-vivo* pharmacokinetic study shows, for instance, that the current intensity can affect the area under the curve (AUC) and the steady-state plasma concentration [21]. Under the conditions of the study, *in-vitro* steady-state skin permeation flux of naloxone rises with the concentration of naloxone hydrochloride dehydrate [21]. Because $J(\infty)$ remains the same whether or not the skin is rate-limiting, the approximation is not expected to affect the choice of the dose used for a particular treatment. However, when the exposure, measured by AUC, is considered, it is important to use the correct plasma drug concentration-time profile. Miscalculation of AUC may lead to under or over-exposure to a drug.

The IVIVC described may be implemented to gauge the *in-vivo* performance of iontophoretic devices and to predict the time course of the plasma concentration based on the *in-vitro* data. In most cases, the steady-state flux is applied to calculate the *in-vivo* plasma concentrations using one- or two-compartmental models [22]. This study provides additional tools to preclinical researchers to help them decide whether the assumption of a constant flux model is justified. In addition, the mathematical models and closed-form solutions will facilitate the design of simulation experiments. Once the iontophoretic transport parameters are identified from *in-vitro* experiments, mean pharmacokinetic data from the literature will be collected to help optimize *in-vivo* iontophoretic delivery. For example, the influence of the current application time can be investigated.

4.3. Analysis and generalization of the method

For a one-compartment model, the analysis is centered on the expression for $\bar{C}_p(s)$ (Eq. (25)) which combines the single time constant from the one-compartment model $1/k_e$ with an infinite number of time constants from the skin $4h^2/(4Dn^2\pi^2 + D\nu^2)$, where n varies from 1 to ∞. After replacing the transport dynamics in the skin by the effective time constant $t_{eff,sk}$, we have $t_{c,1} = 1/k_e \gg t_{eff,sk}$, i.e. $t_{c,1} > 10 \times t_{eff,sk}$ for practical purposes:

$$\frac{1}{k_e} > \frac{10 \times h^2(3\nu^2 - 2sinh(\nu)\nu + (\nu^2 - 4)cosh(\nu) + 4)}{2D\nu^2(2 - 2cosh(\nu) + \nu sinh(\nu))} \tag{51}$$

When Eq. (51) holds, $\bar{J}(s) \simeq J(\infty)/s$ and

$$C_p(t) \simeq \frac{J(\infty)A}{k_e V}(1 - e^{-k_e t}) \tag{52}$$

Therefore, $\lim_{t_{c,1}/t_{eff,sk}\to\infty}(ISE) = 0$. Eq. (52) becomes inaccurate when $t_{c,1} \leq 10 \times t_{eff,sk}$ because $\bar{J}(s)$ can no longer be estimated by $J(\infty)/s$. When $t_{c,1} = 10 \times t_{eff,sk}$, we have $ISE = 0.15$ (Fig. 2).

A similar examination of the drug concentration in the central compartment of a two-compartment model shows that $\bar{C}_1(s)$(i.e., Eq. (35)) is dominated by the contribution of second-order kinetics from the elimination model and the dynamics of drug transport across the skin. The condition $t_{c,2} = (k_{12}^2 + 2k_{12}k_{21} + k_{21}^2 + k_{12}k_e)/(k_{21}^2 k_e + k_{12}k_{21}k_e) \gg t_{eff,sk}$ is imposed after using a single time constant to indicate clearance of the medicine from the body ($t_{c,2}$). Similar to the analysis for the one-compartment model, we have $t_{c,2} > 10 \times t_{eff,sk}$:

$$\frac{k_{12}^2 + 2k_{12}k_{21} + k_{21}^2 + k_{12}k_e}{k_{21}^2 k_e + k_{12}k_{21}k_e} > \frac{10 \times h^2(3\nu^2 - 2sinh(\nu)\nu + (\nu^2 - 4)cosh(\nu) + 4)}{2D\nu^2(2 - 2cosh(\nu) + \nu sinh(\nu))} \tag{53}$$

and $\lim_{t_{c,2}/t_{eff,sk}\to\infty}(ISE) = 0$. In this case, C_1 is represented by

$$C_1(t) = -\frac{J(\infty)Ae^{-\frac{1}{2}t(k_e+k_{12}+k_{21}+\phi)}}{2V_1 k_e \phi}\Big(-2\phi e^{\frac{1}{2}t(k_e+k_{12}+k_{21}+\phi)} - k_e e^{t\phi} + k_e + k_{12}e^{t\phi} + k_{21}e^{t\phi} - k_{12} - k_{21} + \phi e^{t\phi} + \phi\Big) \tag{54}$$

where

$$\phi = \sqrt{(k_e + k_{12} + k_{21})^2 - 4k_{21}k_e} \tag{55}$$

Eq. (54) not applicable when $t_{c,2} \leq 10 \times t_{eff,sk}$ because $\bar{J}(s) \neq J(\infty)/s$. When $t_{c,2} = 10 \times t_{eff,sk}$, we have $ISE = 0.24$ (Fig. 5).

5. Conclusions

A new methodology, based on first-principles modeling, was adopted to estimate *in-vivo* data from *in-vitro* transdermal iontophoretic delivery. Closed-form solutions for the plasma drug concentrations in a one- and two-compartment open model were derived using Laplace transforms. This research also developed expressions for calculating time constants for the steady-state transdermal flux and plasma drug concentration. Given individual PK parameter values, medication blood levels can be predicted using transient release rate profiles from *in-vitro* investigations. The equilibrium flux is adequate only in cases where the ratio of time constants in the skin to the blood compartment is far greater than unity. Simulations, using iontophoretic and pharmacokinetic parameters of amitriptyline (HCl) as references, show that the blood concentration and the time constant decreased with an increase in the elimination rate constant. A study that focused on a two-compartment model for dexamethasone sodium-m-sulfobenzoate yielded similar results. The approach was tested on a growth-hormone releasing factor administered to hairless guinea pigs and naloxone given to rats.

Supplementary Materials

Supplementary material associated with this article can be found, in the online version, at doi:10.1016/j.mbs.2015.10.011.

References

[1] M. Kaur, K.B. Ita, I.E. Popova, S.J. Parikh, D.A. Bair, Microneedle-assisted delivery of verapamil hydrochloride and amlodipine besylate, Eur. J. Pharm. Biopharm. 86 (2014) 284–291.

[2] B.E. Polat, D. Hart, R. Langer, D. Blankschtein, Ultrasound-mediated transdermal drug delivery: mechanisms, scope, and emerging trends, J. Control Release 152 (2011) 330–348.

[3] T. Gratieri, Y.N. Kalia, Targeted local simultaneous iontophoresis of chemotherapeutics for topical therapy of head and neck cancers, Int. J. Pharm. 460 (2014) 24–27.

[4] B.Z. Wang, H.S. Gill, C. He, C. Ou, L. Wang, Y.C. Wang, H. Feng, H. Zhang, M.R. Prausnitz, R.W. Compans, Microneedle delivery of an M2e-TLR5 ligand fusion protein to skin confers broadly cross-protective influenza immunity, J. Controlled Release 178 (2014) 1–7.

[5] A. Djabri, R.H. Guy, M.B. Delgado-Charro, Transdermal iontophoresis of ranitidine: an opportunity in paediatric drug therapy, Int. J. Pharm. 435 (2012) 27–32.

[6] F.T. Vicentini, L.N. Borgheti-Cardoso, L.V. Depieri, D. de Macedo Mano, T.F. Abelha, R. Petrilli, M.V. Bentley, Delivery systems and local administration routes for therapeutic siRNA, Pharm. Res. 30 (2013) 915–931.

[7] K.B. Ita, A.K. Banga, In vitro transdermal iontophoretic delivery of penbutolol sulfate, Drug Deliv. 16 (2009) 11–14.

[8] A.K. Nugroho, O. Della Pasqua, M. Danhof, J.A. Bouwstra, Compartmental modeling of transdermal iontophoretic transport: I. In vitro model derivation and application, Pharm. Res. 21 (2004) 1974–1984.

[9] A.K. Nugroho, O. Della-Pasqua, M. Danhof, J.A. Bouwstra, Compartmental modeling of transdermal iontophoretic transport II: in vivo model derivation and application, Pharm. Res. 22 (2005) 335–346.

[10] P. Singh, M.S. Roberts, H.I. Maibach, Modelling of plasma levels of drugs following transdermal iontophoresis, J. Controlled Release 33 (1995) 293–298.

[11] J.C. Keister, G.B. Kasting, Ionic mass transport through a homogeneous membrane in the presence of a uniform electric field, J. Membr. Sci. 29 (1986) 155–167.

[12] K. Tojo, Mathematical Models of Transdermal and Topical Drug Delivery, second ed., Biocom Systems, Fukuoka, Japan, 2005.

[13] R. Collins, The choice of an effective time constant for diffusive processes in finite systems (Thermal conduction and sputtering examples), J. Phys. D: Appl. Phys. 13 (1980) 1935.
[14] K. Tojo, Mathematical model of iontophoretic transdermal drug delivery, J. Chemical Eng. Japan 22 (1989) 512–518.
[15] L. Simon, Timely drug delivery from controlled-release devices: dynamic analysis and novel design concepts, Math. Biosci. 217 (2009) 151–158.
[16] L. Simon, A.N. Weltner, Y. Wang, B. Michniak, A parametric study of iontophoretic transdermal drug-delivery systems, J. Membrane Sci. 278 (2006) 124–132.
[17] P. Schulz, P. Dick, T.F. Blaschke, L. Hollister, Discrepancies between pharmacokinetic studies of amitriptyline, Clinical Pharm. 10 (1985) 257–268.
[18] L.L. Ferry, G. Argentieri, D.H. Lochner, The comparative histology of porcine and guinea pig skin with respect to iontophoretic drug delivery, Pharm. Acta. Helv. 70 (1995) 43–56.
[19] S. Kumar, H. Char, S. Patel, D. Piemontese, A.W. Malick, K. Iqbal, E. Neugroschel, C.R. Behl, In vivo transdermal iontophoretic delivery of growth hormone releasing factor GRF (1–44) in hairless guinea pigs, J. Controlled Release 18 (1992) 213–220.
[20] G. Hochhaus, J. Barth, S. al-Fayoumi, S. Suarez, H. Derendorf, R. Hochhaus, H. Möllmann, Pharmacokinetics and Pharmacodynamics of Dexamethasone Sodium-m-Sulfobenzoate (DS) after Intravenous and Intramuscular Administration: A Comparison with Dexamethasone Phosphate (DP), J. Clinical Pharm. 41 (2001) 425–434.
[21] R. Yamamoto, S. Takasuga, Y. Yoshida, S. Mafune, K. Kominami, C. Sutoh, Y. Kato, M. Yamauchi, M. Ito, K. Kanamura, M. Kinoshita, In vitro and in vivo transdermal iontophoretic delivery of naloxone, an opioid antagonist, Int. J. Pharm. 422 (2012) 132–138.
[22] D.M. Chilukuri, G. Sunkara, D. Young, Pharmaceutical Product Development : In Vitro-In Vivo Correlation, Informa Healthcare, New York, 2007.